High-energy polarized electron beams from the ionization of isolated spin polarized hydrogen atoms

Dimitris Sofikitis , ^{1,*} Lars Reichwein , ^{2,3} Marios G. Stamatakis , ⁴ Christos Zois , ¹ Dimitrios G. Papazoglou , ^{5,6} Samuel Cohen , Markus Büscher, Alexander Pukhov, and T. Peter Rakitzis ¹Department of Physics, Atomic and Molecular Physics Laboratory, University of Ioannina, University Campus, Ioannina, GR-45110, Greece ²Institut für Theoretische Physik I, Heinrich-Heine-Universität Düsseldorf, 40225 Düsseldorf, Germany ³Peter Grünberg Institut (PGI-6), Forschungszentrum Jülich, 52425 Jülich, Germany ⁴Department of Mathematics, University Campus, Ioannina, GR-45110, Greece ⁵Materials Science and Engineering Department, University of Crete, GR 70013, Heraklion, Greece ⁶Institute of Electronic Structure and Lasers, Foundation for Research and Technology-Hellas, 71110 Heraklion-Crete, Greece ⁷Institut für Laser- und Plasmaphysik, Heinrich-Heine-Universität Düsseldorf, 40225 Düsseldorf, Germany ⁸Department of Physics, University of Crete, 70013 Heraklion-Crete, Greece

(Received 8 March 2024; revised 25 April 2025; accepted 5 May 2025; published 28 May 2025)

We propose a laser-based method for the preparation of high-energy polarized electrons, from the ionization of isolated spin polarized hydrogen (SPH) atoms. The SPH atoms are prepared from the photodissociation of hydrohalide molecules, using two consecutive UV pulses of ps duration. By appropriately timing and focusing the pulses, we can spatially separate the highly polarized SPH from other unwanted photoproducts, which then act as the target for the acceleration lasers. We show how elastic collisions define number density n and polarization P regimes for the prepolarized targets, and use particle-in-cell simulations to demonstrate the method's feasibility.

DOI: 10.1103/PhysRevA.111.053119

I. INTRODUCTION

Polarized electron and positron beams are powerful experimental tools, used in a diverse set of disciplines, ranging from studies of atomic and molecular structure [1,2] and material science [3,4], to nuclear and high-energy physics [5], where electrons accelerated to relativistic energies can be used to test new physics beyond the standard model [6-8]. Producing intense beams of highly polarized, high-energy electrons can be done using conventional acceleration methods involving accumulation in storage rings [9,10], as well as emerging methods involving filtering of polarized electrons [11,12]. Alternatively, high-energy polarized electrons can be produced using polarized photocathodes [13,14], or through laser ionization of noble gases [15–17].

Laser-plasma based acceleration of electrons [18], combined with recent laser methods for the preparation of high-density SPH [19–21], open a new potentiality for ordersof-magnitude higher electric currents: that of accelerating electrons resulting from the ionization of prepolarized targets. Following this, a variety of recent proposals predict the production of high-energy spin-polarized electron beams utilizing such targets [22-25], predicting up to kA electric currents [23].

The direct use, however, of such SPH atoms as targets for electron acceleration is limited by several factors. The presence of the halide atoms means that their valence electrons (which are only weakly polarized by the photodissociation) and inner-shell electrons (which are unpolarized) are also liberated and accelerated, lowering the total polarization of the accelerated electrons to very low values. It could be possible to ionize the halide atom and subsequently remove the ions using electric fields [25], however, this is quite challenging to achieve within the timescales required for laser acceleration. Finally, dissociation of H₂ molecules at wavelengths below 100 nm, which would not suffer any halide atom presence, has not been experimentally tested and the percentage of direct molecular ionization has not been evaluated [23].

Additionally, the SPH polarization depends on the parent molecule bond orientation, resulting in a $\cos^2\theta$ spatial distribution of the polarization, a fact that sets an upper limit for the free-space value for polarization of 40%. Bond orientation, which can lift this limitation, can be achieved using a strong IR pulse. However, apart from the complication or using an extra pulse of different wavelength (MIR), bond alignment cannot be 100% successful for moderate IR pulse intensities needed to avoid unwanted multiphoton or even field ionization effects. Finally, the hyperfine structure of hydrogen atoms causes the polarization to oscillate from the electron to the proton and backwards, with a period of 0.7 ns, meaning that any manipulation aimed to removing the unwanted halide atoms or to achieving bond orientation, has to be synchronized with this oscillation to avoid further reduction of electron polarization. Proposed solutions lead to experimental complications, ultimately limiting the method's feasibility.

Here, we propose a simple and intuitive method, which circumvents all the limitations mentioned above. The method takes advantage the kinematics of the dissociation process, the angular distribution of the polarization of the atomic fragments and the shape of the dissociation laser beams, to produce pure targets of highly polarized SPH, without the presence of the unwanted halide partners.

^{*}Contact author: sofdim@uoi.gr

In the next paragraphs, we describe the proposed method and use a numerical model to predict the density and polarization of the SPH atoms in the target, as a function of time and in the absence of collisions, resulting from the photodissociation of HCl, HBr, and HI at 213 nm. Next, we describe how elastic collisions define the polarization-density-dimensions regimes and describe the effect of elastic collisions on the density and polarization of the SPH target. Finally, we use particle-in-cell (PIC) simulations to demonstrate the feasibility of laser acceleration with these isolated SPH targets.

II. THEORY

A. Pulse sequence for isolating the SPH atoms

In the first step, we illuminate a hydro-halide sample using a focused UV laser to dissociate all molecules within the laser focus and along the Rayleigh range of the laser beam. The halogen and H atomic fragments will acquire large velocities, that will cause them to exit this volume within a few tens of ns, creating a volume devoid of atoms or molecules, hereafter referred to as hole. In the second step, a second dissociation pulse of larger spatial dimensions (but of same wavelength and pulse duration as the first), dissociates molecules in a larger volume around the hole, hereafter called the reservoir. SPH atoms will now fly from the reservoir to the hole volume (much faster than the heavier halogen atoms), where they can be ionized to produce accelerated electrons by an acceleration pulse in the third step. The narrow velocity distributions of the fragments and the available dissociation laser beam geometries allow tailoring the hole and reservoir geometries, so that, in the third step, only hydrogen atoms of high polarization are contained inside the hole.

We consider dissociation pulses 1 (DP1) and 2 (DP2), of the same wavelength and duration (around 200 nm and 100 ps for example), but with different spot size, intensity, and synchronization. The pulses are directed towards a molecular beam containing, for example, HCl molecules (Fig. 1). The molecular beam moves with a velocity around 1000 m/s perpendicular to the direction of propagation of the dissociation pulses; for simplicity, we use the reference frame of the moving molecular beam.

At t = 0, the pulse DP1 will dissociate all HCl molecules in the volume of the hole, which is shaped as a prolate ellipsoid, with semiaxes a, b (\approx 10 µm), and c, which are parallel to x, y, and z axes, respectively. We choose the Rayleigh range to be larger than the width of the molecular beam; this way, the hole is truncated, i.e., the front and back ends of the ellipsoid defining the hole are cut, and consequently no HCl molecules are in front or after the area of the target. Dissociating HCl at $\lambda = 200$ nm results in H atoms with speed $v_H \approx 17$ km/s and Cl atoms with speed $v_{\rm Cl} \approx 0.47$ km/s [Fig. 1(b)]. Thus, the H atoms will leave the volume of the hole in a few ps, and subsequently, the Cl atoms will also exit in few tens of ns, leaving the volume of the hole devoid of atoms and molecules. After \approx 45 ns, DP2 can be fired, which will produce fast SPH atoms in the reservoir, which will then rapidly fill the hole after \approx 1.42 ns (twice the hyperfine beating time).

Following dissociation, fast moving SPH atoms move towards all directions, with a large number of them ending up

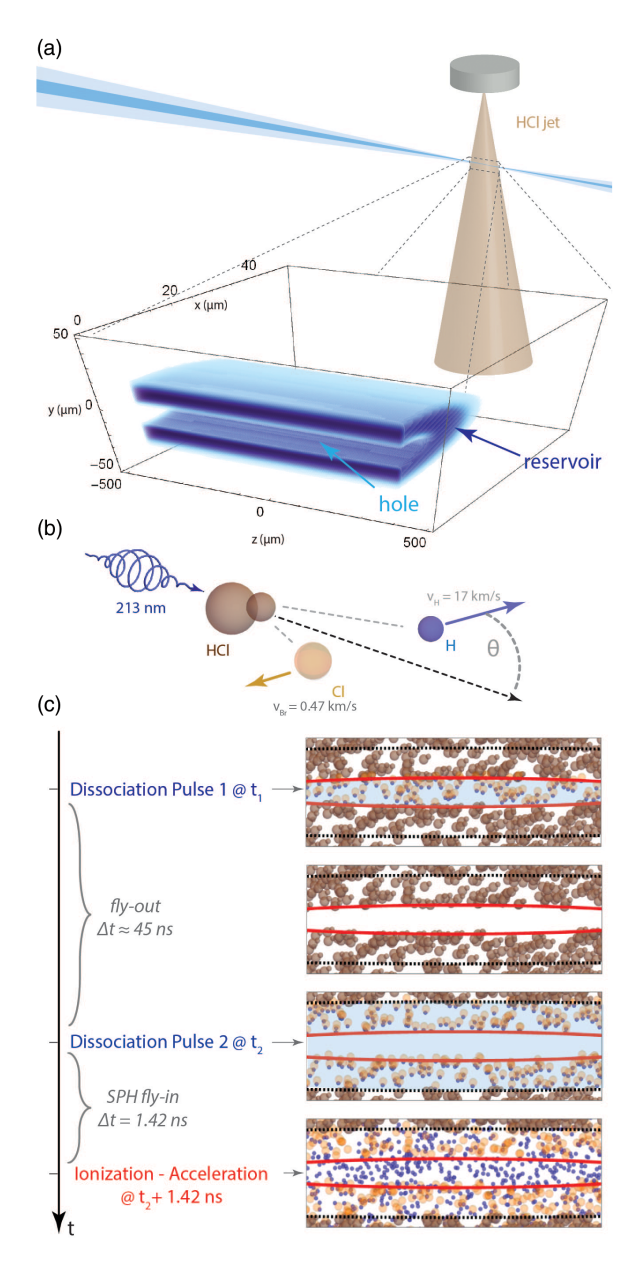


FIG. 1. (a) Experimental setup, showing the gas jet and laser beams. (b) Velocities associated with the dissociation process. (c) The stages of the experiment: (i) complete photodissociation only in area of hole; (ii) hole empties of atoms; (iii) complete photodissociation in reservoir around hole; (iv) hole fills with SPH.

in the volume of the hole. The polarization of these atoms depends on their recoil angle: ns laser dissociation of HCl results in narrow velocity distributions for the atomic fragments [26]. For dissociation at $\lambda=213$ nm, the velocity distribution is a function of the angle θ , while the polarization of the SPH atoms along the z direction is also a function of θ . In both cases, θ is the apex angle used in spherical coordinates [shown in Fig. 1(b)], i.e., the dissociation laser beams propagate parallel to the z axis with $\theta=0$. Note that, following dissociation, the polarization of the SPH atoms oscillates due to coupling with the nuclear spin (1/2 for the proton), via the hyperfine interaction [20], as shown in Fig. 3(a). So, in general, the SPH polarization depends on (i) emission angle and (ii) time, given by $P_{\rm HF}(t)$ [shown in Fig. 3(a)]. We refer to the emission-

angle polarization as geometric polarization (P_G), and the total (observable) polarization as $P_{\text{tot}} = P_G \times P_{\text{HF}}(t)$.

B. Geometrical polarization P_G

When an HI, an HBr, or an HCl molecule is photodissociated using circularly polarized light at $\lambda = 200$ nm, the recoil probability and polarization distribution are given by [26,27]:

$$I(\theta) = N\left(1 + \frac{1}{2}P_2(\cos\theta)\right) \tag{1}$$

with $P_2(x)$ being the second Legendre polynomials and N a normalization factor. The polarization of the SPH atoms along the z direction is:

$$P(\theta) = \cos^2 \theta. \tag{2}$$

To acquire the overall geometrical polarization of a large sample of H atoms generated using UV photodissociation, we need to integrate the product of these distributions over all space, and divide with the number of atoms. Since the recoil distribution and the polarization solely depend on the polar angle θ , P_G will be:

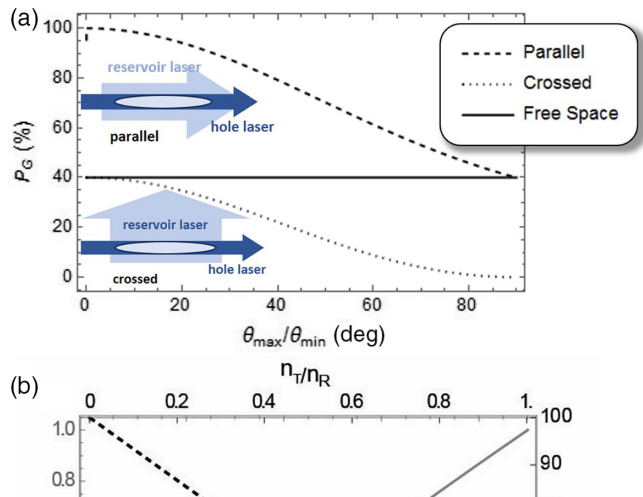
$$P_{G} = \frac{\int_{\theta_{\min}}^{\theta_{\max}} P(\theta) I(\theta) \sin\theta d\theta}{\int_{\theta_{\min}}^{\theta_{\max}} I(\theta) \sin\theta d\theta},$$
 (3)

where θ_{\min} and θ_{\max} are the limiting angles for the integration $(0 \le \theta_{\max}, \theta_{\min} \le \pi)$. By setting $\theta_{\min} = 0$ and $\theta_{\max} = \pi$ for example, one easily obtains the free-space value of 40%.

If, however, free space can be tailored, for example by choosing particular geometries for the volume from which H atoms originate and accumulate to, as is done here, the limiting angles can change, and so will P_G . It is easy to show that the photodissociation geometries used, where the hole and reservoir lasers propagate in the same direction, the limiting angle θ_{min} will remain constant and equal to zero while θ_{max} will vary from zero to $\pi/2$ as a function of loading time. Conversely, θ_{\min} will vary with time and θ_{\max} will remain constant and equal to $\pi/2$ if instead of a parallel, a crossed orientation is chosen between the hole and reservoir beams [parallel and crossed schemes shown in the insets of Fig. 2(a)]. In Fig. 2(a) we show the evolution of P_G as a function of either $\theta_{\rm max}$ (parallel case) and $\theta_{\rm min}$ (crossed case), as well as the free-space value. We see that choosing the parallel geometry allows for polarization maximization for small values of the limiting angle θ_{max} .

This, of course, comes with the expense of reducing the density of the sample, since now, entire directions of space are removed from contributing to the sample density in the hole. The density as a function of θ_{max} in the parallel case is shown in Fig. 2(b) (gray curve, left and lower axis). Regardless of any specific geometrical arrangements, the maximum density (as a percentage of the initial density of the parent molecule) for which a specific polarization can be achieved is shown in Fig. 2(b) (dashed black curve, right and upper axis).

The detailed numerical model, which takes into account the geometry of the hole and reservoir, (including the laser intensity profile, or the hole and reservoir truncation due to the limited size of the molecular beam) calculates the density



(b) 0 0.2 0.4 0.6 0.8 1. 100
90
80
70 80
70 80
60
60
θ_{πεκ} (deg)

FIG. 2. (a) Evolution of P_G as a function of θ_{\max} (parallel case) and θ_{\min} (crossed case) and free space value. (b) Evolution of the target density n_T , as a fraction of the initial density of the parent molecules, with respect to the evolution of the limiting angle θ_{\max} for the parallel case (gray curve, left and lower axis). Geometric polarization P_G as a function of the density inside the hole in the parallel case (dashed black curve, right and upper axis).

of the target at a function of time as:

$$n_T = \frac{\int_0^\pi \int_0^{2\pi} I(\theta) V(\theta, \phi, t) \sin\theta d\theta d\phi}{\int_0^\pi \int_0^{2\pi} I(\theta) \sin\theta d\theta d\phi}$$
(4)

while the target polarization as

$$P_{T} = \frac{\int_{0}^{\pi} \int_{0}^{2\pi} P(\theta)I(\theta)V(\theta, \phi, t)\sin\theta d\theta d\phi}{\int_{0}^{\pi} \int_{0}^{2\pi} I(\theta)V(\theta, \phi, t)\sin\theta d\theta d\phi}$$
(5)

while

$$V(\theta, \phi, t) = H(\hat{r})R(\hat{r} + \vec{v}t) \tag{6}$$

is the time-dependent volume defined by the overlap of the volumes of the hole $H(\hat{r})$ and the reservoir $R(\hat{r} - \vec{v}t)$ at a given direction, without considering collisions [28]. If we consider one collision per atom at $t = t_{\rm cft}$ (with $t_{\rm cft} = l_{\rm mfp}/v_H$ with $l_{\rm mfp}$ being the collision mean-free path and v_H the speed of the H atoms), then instead of $V(\theta, \phi, t)$, one must consider

$$V^{\text{coll}}(\theta, \phi, t) = \int_0^{\pi} \int_0^{2\pi} H(\hat{r}) R'[\hat{r} + \vec{v}t_{\text{cft}} + \vec{v}'(t - t_{\text{cft}})] d\theta' d\phi'$$
(7)

with $R'(\hat{r}) = R(\hat{r} + \vec{v}t_{\rm cft})[1 - H(\hat{r})]$ being the volume of the reservoir atoms, which have not entered the target area before $t_{\rm cft}$.

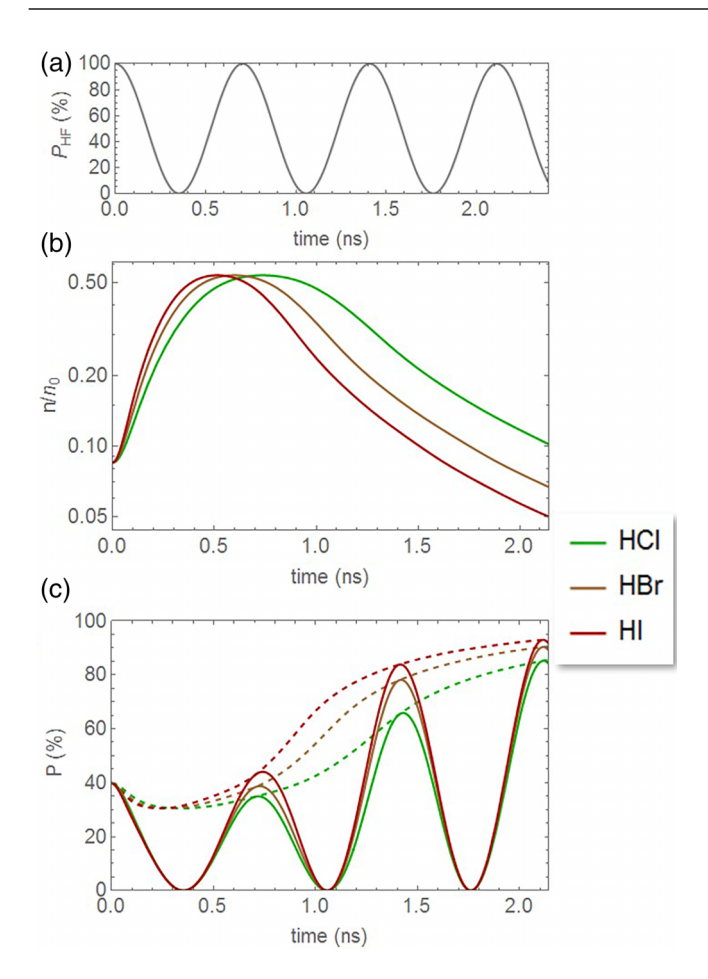


FIG. 3. (a) Polarization evolution of the hydrogen electron due to the hyperfine interaction. (b) Density of SPH atoms target atoms n_T inside the hole, over the initial density of the reservoir n_R , as a function of time after firing DP2, in the absence of collisions. (c) P_G (dashed lines) and total polarization (solid lines) of the hydrogen atoms inside the hole as a function of time after firing the DP2, again, in the absence of collisions.

III. RESULTS AND DISCUSSION

We can simulate the preparation of an isolated SPH target; we choose to employ 213 nm pulse to create a target of moderate width of around 20 μ m, and we choose to explore employing HCl, HBr, and HI dissociation. We exclude HF from our considerations, since the photodissociation cross section is very small for this molecule at 213 nm, and while it has been shown theoretically that HF gives SPH from photodissociation near 157 nm [29], the feasibility of the photodissociation process has not been experimentally demonstrated.

In Fig. 3(b), we see the ratio of the target density n_T of the SPH entering the hole over the initial density of the parent molecules in the reservoir n_R , as a function of time after firing DP2, in the absence of collisions (green, brown, and red lines correspond to the dissociation of HCl, HBr, and HI, respectively). The density of the SPH atoms rises fast, reaching close to half the initial density of the parent molecules in the molecular beam at $t \approx 0.5$ ns, and afterwards is gradually reduced.

In Fig. 3(c), we show the values for P_G (dashed lines) and P_{tot} (solid lines) as a function of time. We see that the P_G curve starts around 40% (the free-space value), and increases to $\approx 80\%$ at t ≈ 2 ns. This polarization increase is to be expected: the hole is shaped as a prolate ellipsoid with its large axis parallel to the laser propagation. SPH atoms recoiling at large angles with respect to the laser propagation axis have low polarization $[P(\theta \approx \pi/2) \approx 0]$, and exit the hole very quickly. In contrast, highly polarized SPH atoms with small recoil velocities stay in the hole longer, since they transverse a much larger distance to exit [28].

In Fig. 3(c) we see that the electron polarization is maximized at t=0.7 ns, i.e., the hyperfine period of the electron-proton system and all integer multiples of this time. For the case of HCl dissociation, the overall electron polarization at t=1.42 ns is close of 70% with a loss of a factor of $\approx 1/5$ in density [shown in Fig. 3(b)], while at t=2.12 ns the polarization surpasses 80%, with an almost double corresponding reduction in density. If instead of HCl, HBr, or HI photodissociation is considered, the resulting polarization can reach more than 75% and 80%, respectively. Note that the solid curve reaches zero at t=0.35 ns (half the hyperfine period for the electron-proton system) and integer multiples of this time. At this point all polarization is transferred to the proton nuclear spin, offering a target for laser acceleration of polarized protons.

A. Limitations due to elastic collisions

The maximum density in which such a prepolarized target can be prepared is limited by elastic collisions. Note that depolarizing H-halogen collisions are negligible in comparison, as the H-Cl depolarizing cross section has been measured to be orders of magnitude smaller than the corresponding elastic collision cross section [30]. However, even nondepolarizing collisions, change the SPH recoil trajectories and ultimately break the correlation between the recoil angle and polarization.

We estimate the number of elastic collisions by considering the collisions mean-free path $l_{\rm mfp}$ and the mean-free time between collisions $t_{\rm fct}$. We can calculate the time it takes for the last SPH atom coming from the reservoir to exit the hole, and compare it to $t_{\rm cft}$. More generally, by setting $t_{\rm ex}^{\theta_{\rm max}}=1.5\times t_{\rm cft}$ we obtain $a\approx \frac{\sin\theta_{\rm max}}{(1+q)^{\frac{2n}{2}}}$, with a being the small axis of the ellipsoid defining the hole, σ the collision cross section, n_R the density of the parent molecules in the molecular beam, and q the ratio $\frac{a_R}{a}$ of the diameter a_R of the reservoir laser PD2 over the diameter of laser PD1. In this way one can obtain the lines shown in Figs. 4(a), 4(c) and 4(e), for the dissociation of HCl, HBr, and HI, respectively, while combining with Eq. (5) we can obtain the lines shown in Figs. 4(b), 4(d) and 4(f), again for the dissociation of HCl, HBr, and HI, respectively.

The target density and polarization depend both on the size and the angular dependence of the elastic collision differential cross section (DCS) [31]. We have found that for an isotropic DCS, a useful rule of thumb for estimating the target polarization as a function of its density and dimensions is to set the density so that $t_{\rm acc} \approx 1.5 \times t_{\rm cft}$, an arrangement that keeps collisional depolarization limited to the outer parts of the target. The target diameter, density and polarization

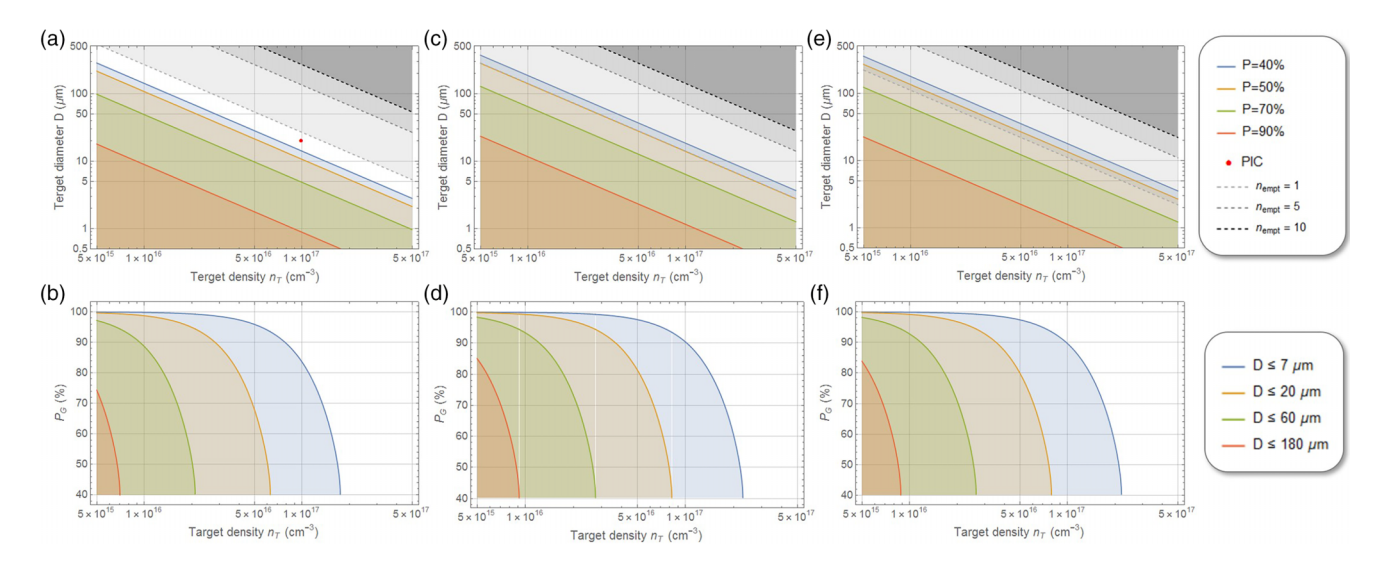


FIG. 4. (a) Maximum SPH prepolarized target diameter as a function of the target density, for the photodissociation of HCl at 213 nm, for various degrees of polarization. The red dot shows the conditions in which PIC simulations were performed. (b) Maximum polarization as a function of density for various choices for the target diameter D, again, for the photodissociation of HCl at 213 nm. (c) and (e) Similar to (a) but for the photodissociation of HBr and HI at 213 nm, respectively. (d) and (f) Similar to (b) but but for the photodissociation of HBr and HI at 213 nm, respectively.

regimes resulting such a criterion are shown in Fig. 4. The maximum target diameter at a given density and polarization is approximately inversely proportional to the total elastic collision cross section. When the target polarization is chosen to be close to the thermal value of 40%, the criterion $t_{\rm acc} \approx 1.5t_{\rm cft}$ can be relaxed even further to allow a few consecutive collision events.

For a target polarization around of 40%, the target polarization no longer limits its size; however, new limitations arise from collisions during the first step, that of creating the hole using DP1. In this step, only halogen-to-halogen elastic collisions can delay the emptying process by forcing the halogen atoms into a random walk. This weak limitation is visualized using the gray dashed lines in Figs. 4(a), 4(c) and 4(d), which mark the onset of one, five, and ten average halogen collisions during the step of emptying the hole using DP1.

We can choose to simulate the preparation of a $\approx\!20\,\mu m$ wide target, using HCl dissociation at 213 nm. The H-H polarized elastic collision cross section is calculated to be around $\sigma_{\text{H-H}}\approx130$ a.u. [31–33], while an additional elastic collision cross section $\sigma_{\text{H-Cl}}\approx160$ a.u., related to elastic H-Cl collisions is expected.

In Fig. 5(a), we show with the solid gray line, the target density n_T at $t_{\rm acc} = 1.42$ ns, when the reservoir density (i.e., the initial density of the molecular beam) has been chosen to be $n_R = 8 \times 10^{16}$ cm⁻³. This density corresponds to $l_{\rm mfp} \approx 17$ µm and $t_{\rm fct} \approx 1$ ns. Looking at Fig. 3(b), we see that by this time, the maximum density inside the hole has been reached, and it is starting to decline. This means that the by this time, most of the atoms will have entered the area of the hole, which lies in a lower density, and therefore they will experience almost no collisions. The evolution of the density

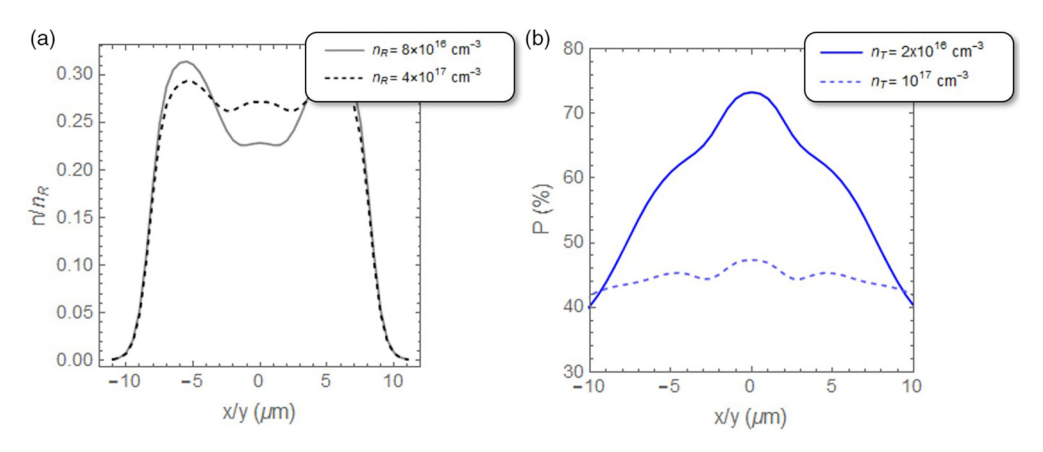


FIG. 5. (a) Density distribution of the target SPH atoms n_T at t = 1.42 ns, for $n_R = 4 \times 10^{17}$ cm⁻³(solid gray line) and $n_R = 8 \times 10^{16}$ cm⁻³ (dashed black line). (b) Polarization distribution of the target SPH atoms at t = 1.42 ns, at $n_T = 10^{17}$ cm⁻³ (solid blue line) and $n_T = 2 \times 10^{16}$ cm⁻³ (dashed blue line).

inside the hole will mostly resemble the one shown in Fig. 3(b) where no collisions have been taken into account. Similarly, the polarization, shown in Fig. 5(b) with the blue solid line, will have an evolution similar to what is shown in Fig. 3(c), as only few atoms in the borders of the hole will have been affected by collisions.

If we assume however a higher density, for example equal to $n_R = 4 \times 10^{17} \ {\rm cm^{-3}}$, then $l_{\rm mfp} \approx 3.5 \ \mu {\rm m}$ and $t_{\rm fct} \approx 0.2 \ {\rm ns}$. At this time, most SPH atoms will still be outside the volume of the hole, and therefore collisions have to be taken into account. Collisions randomize the emission direction and while they do not significantly change the density fraction of the atoms ending up in the hole at $t_{\rm acc} = 1.42 \ {\rm ns}$, [shown in Fig. 5(a) with a dashed black line], the polarization has been almost totally randomized and reduced to near its free-space value of 40%, as we see in Fig. 5(b) with the dashed blue line. Note that both the density and the polarization distributions are homogenized in direction z, the laser propagation direction, for most of the target's length.

B. PIC simulations

To investigate wake-field acceleration of polarized electrons with such targets, we conduct two-dimensional PIC simulations with the code VLPL [34,35]. The simulations utilize a grid resolution of $h_x = 0.02\lambda$, $h_y = 0.05\lambda$. As we utilize the rhombi-in-plane Maxwell solver [36], the time step is chosen as $\Delta t = h_x/c$. The wavelength of the driving laser, which is the normalization constant for our simulations, is chosen as $\lambda = 1.6 \, \mu m$. Wake fields driven by CO₂ laser pulses or pulses in the midinfrared range have been the subject of several theoretical studies such as Refs. [37,38] showing that self-trapping at lower plasma densities can be achieved, making use of the fact that the threshold for self-trapping in wake fields depends on the critical density, which is lower for larger wavelengths.

We model our target as a slab, consisting of Gaussian-shaped HCl walls with a density of 3.5×10^{17} cm⁻³ and a central channel containing the spin polarized hydrogen (and electrons), at a density of 10^{17} cm⁻³ and a channel width of 20 μ m. For simulation purposes, we choose a target length of 240 μ m and consider the SPH as being preionized (potential spin-dependent effects during ionization are discussed *inter alia* in Ref. [39]). The electrons are prepolarized in *z* direction.

We use a driving pulse (moving in +z direction) with $a_0 = 6$, focal spot size of 3λ and a duration of $6\lambda/c$. As shown in Fig. 6, polarized electrons are guided and accelerated in the channel structure induced by the laser pulse. Due to targetry restrictions, the choice of laser parameters is rather limited: while stronger pulses are of interest for self-trapping, higher intensity will lead to increased spin precession and a loss of polarized electrons to the HCl walls. For the aforementioned laser and target parameters, we are able to accelerate 3.9 pC up to approximately 4 MeV over the target length and up to 48% of the initial target polarization is preserved. Considering an initial polarization around 45% for the isolated SPH target, we result in a final polarization for the accelerated electron of \approx 22%. These electrons can be injected into a second wakefield stage (similar to Refs. [40,41]) in order to obtain higher energies. If the Lorentz factor becomes sufficiently large dur-

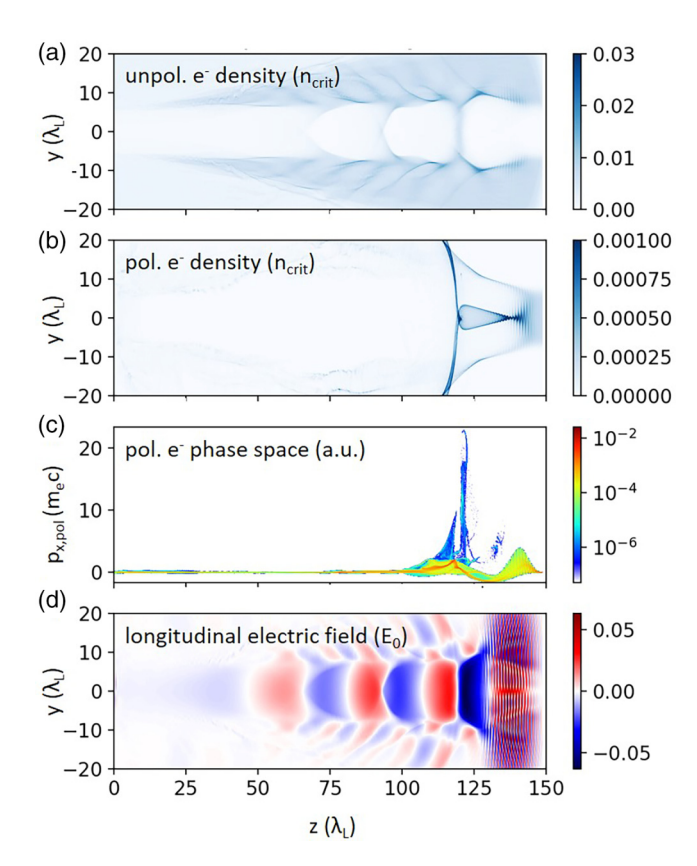


FIG. 6. PIC simulation results. (a), (b) show the unpolarized and polarized electron density, respectively. (c) shows the phase space of only the polarized electrons, while (d) shows the transverse electric field. The color bars are clipped for better visibility.

ing the first stage, the precession of spins according to the T-BMT equation becomes negligible [42].

The laser parameters and injection scheme could be further tuned for different target densities: wider holes of SPH are possible to generate, however, at lower densities, as shown in Fig. 4. One scheme previously proposed for polarized HCl targets has been that of colliding-pulse injection [24,43]. In these theoretical considerations, however, a fully prepolarized target with 10¹⁸ cm⁻³ density and much larger dimensions was used for simulations. Further optimization of this target for wake-field acceleration could consist of implementing density ramps, for example by intensity shaping [44] the reservoir laser beam (see Appendix A). Finally, THz acceleration might offer the possibility of efficient acceleration at lower target densities, due to the scaling of critical density with the acceleration pulse wavelength [45,46], and allow accessing regimes of higher target polarization (see Fig. 4).

IV. CONCLUSIONS

We have shown how, by combining the optical properties and the stereodynamics of the photodissociation process, one can prepare an isolated target of highly polarized SPH atoms, to be used in laser initiated electron acceleration experiments. We have demonstrated how a sample suitable for a simple wake-field acceleration scheme can be prepared to allow MeV energies, which can be brought well into the GeV regime

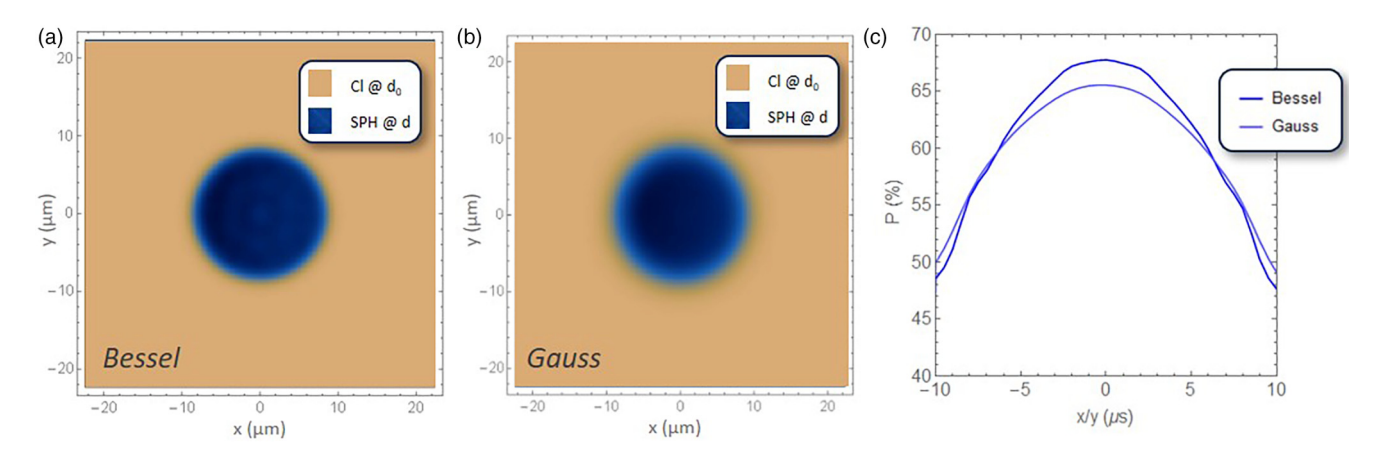


FIG. 7. Cuts of the density distribution inside the hole along the x/y plane, showing contributions from atoms entering the hole at $t \le t_{cft}$ for a normal Gaussian laser (a) and a shaped Bessel beam (b) utilized as PD1. (c) Polarization distribution in the hole at t = 1.42 ns. Comparison between a Besselian and a Gaussian intensity distribution for the photodissociation lasers.

using a subsequent acceleration stage. Owing to the simplicity of the proposed method and the universality of the photodissociation dynamics, a large variety of similar prepolarized targets can be designed to fit the needs of other acceleration schemes.

ACKNOWLEDGMENTS

T.P.R. acknowledges partial financial support by the Hellenic Foundation for Research and Innovation (HFRI) and the General Secretariat for Research and Technology (GSRT), Grant Agreement No. HFRI-FM17-3709 (project NUPOL). The authors gratefully acknowledge the Gauss Centre for Supercomputing e.V. for funding this project (spaf) by providing computing time through the John von Neumann Institute for Computing (NIC) on the GCS Supercomputer JUWELS at Jülich Supercomputing Centre (JSC). The work of A.P. has been supported by BMBF Project. No. 05P24PF1 (Germany).

APPENDIX A: BEAM SHAPING

It is clear that the loading dynamics depend not only on the overall size by also the exact shape of the hole and reservoir. In particular, the shape of the hole-reservoir border depends on the intensity distribution of the dissociating pulses. Laser beams follow Gaussian optics, however, plenty of additional geometries are available through advanced beam intensity-shaping methods. For example, by modulating the spatial spectrum of a Bessel beam [44], we can engineer its intensity profile, achieving a top-hat-like distribution along the propagation direction, and a very narrow, Bessel-like distribution in the transverse direction.

Bessel-like intensity distributions permit sharper holereservoir borders. In Fig. 7(a), we show a slice of the density distribution of SPH inside a hole, using parameters identical to those used in Fig. 3. The parameters used for the calculations shown in Fig. 3(a) correspond to a Besselian intensity distribution, while the ones used in Fig. 3(b) to a usual Gaussian distribution. As we see in Fig. 7(b), the polarization of the target atoms is slightly reduced when a Gaussian laser beam is considered.

Beam shaping can be used as an additional engineering tool to fine tune the method into providing with optimal prepolarized acceleration targets. The potential of using shaped beams seems even greater when considering schemes, which can allow for designing prepolarized targets with nontrivial density distributions, to accommodate advanced plasma-acceleration schemes.

APPENDIX B: MOLECULAR BEAM REQUIREMENTS

The molecular beam requirements can be estimated on the first step, that of emptying the hole, since this is the most time-consuming step in which thermal motion can play a significant role. For a hole such as the main example of the main document, with a width close to 20 µm, the time required after firing PD1 to reduce the density by an order of magnitude is close to 45 ns. Any residual velocity $\Delta v_{x,y}$, due to, for example, thermal motion, will blur the borders between the hole and reservoir, leading to an effect similar to the one discussed in the previous paragraph. If we require for this blur to be at most $0.15 \times a$, with a being the hole ellipsoid small axis, we find $\Delta v_{x,y} = 50$ m/s, corresponding to a translational temperature of around 10 K. This requirement does not change when considering larger diameter for our hole, up to few hundred µm. Note that rotational temperature is irrelevant, and highly polarized SPH and SPD atoms from room-temperature photodissociation have been demonstrated [20]. $\Delta v_{x,y}$ should also take into account the molecular beam divergence: it should remain below $\approx 3^{\circ}$, which, for a molecular beam velocity of ≈ 1000 m/s, corresponds to a spread of 5 cm over the course of one meter.

^[1] J. Kessler, in *Advances in Atomic, Molecular, and Optical Physics* (Elsevier, Amsterdam, 1990), Vol. 27, pp. 81–163.

^[2] T. Gay, Adv. At. Mol. Opt. Phys. 57, 157 (2009).

^[3] J. R. Danielson, D. H. E. Dubin, R. G. Greaves, and C. M. Surko, Rev. Mod. Phys. 87, 247 (2015).

^[4] P. J. Schultz and K. G. Lynn, Rev. Mod. Phys. 60, 701 (1988).

- [5] T. Sun, Q. Zhao, K. Xue, Z.-W. Lu, L.-L. Ji, F. Wan, Y. Wang, Y. I. Salamin, and J.-X. Li, Rev. Mod. Plasma Phys. 6, 38 (2022).
- [6] B. Barish and J. E. Brau, Int. J. Mod. Phys. A 28, 1330039 (2013).
- [7] D. Androić, D. S. Armstrong, A. Asaturyan, T. Averett, J. Balewski, K. Bartlett, J. Beaufait, R. S. Beminiwattha, J. Benesch, F. Benmokhtar *et al.*, Nature (London) 557, 207 (2018).
- [8] B. S. Schlimme, P. Achenbach, C. A. Ayerbe Gayoso, J. C. Bernauer, R. Böhm, D. Bosnar, T. Challand, M. O. Distler, L. Doria, F. Fellenberger *et al.*, Phys. Rev. Lett. 111, 132504 (2013).
- [9] A. Sokolov and I. Ternov, Chomet and edited by CW Kilmister (American Institute of Physics, New York, 1986).
- [10] W. von Drachenfels, F. Frommberger, M. Gowin, W. Hillert, M. Hoffmann, and B. Neff, AIP Conf. Proc. 675, 1053 (2003).
- [11] H. Batelaan, A. S. Green, B. A. Hitt, and T. J. Gay, Phys. Rev. Lett. 82, 4216 (1999).
- [12] M. M. Dellweg and C. Müller, Phys. Rev. Lett. **118**, 070403 (2017).
- [13] D. T. Pierce, F. Meier, and P. Zürcher, Appl. Phys. Lett. 26, 670 (2008).
- [14] J. Maxson, I. Bazarov, B. Dunham, J. Dobbins, X. Liu, and K. Smolenski, Rev. Sci. Instrum. **85**, 093306 (2014).
- [15] I. Barth and O. Smirnova, Phys. Rev. A 88, 013401 (2013).
- [16] Z. Nie, F. Li, F. Morales, S. Patchkovskii, O. Smirnova, W. An, N. Nambu, D. Matteo, K. A. Marsh, F. Tsung *et al.*, Phys. Rev. Lett. 126, 054801 (2021).
- [17] Y.-F. Li, R. Shaisultanov, K. Z. Hatsagortsyan, F. Wan, C. H. Keitel, and J.-X. Li, Phys. Rev. Lett. 122, 154801 (2019).
- [18] T. Tajima and J. M. Dawson, Phys. Rev. Lett. 43, 267 (1979).
- [19] T. P. Rakitzis, P. C. Samartzis, R. L. Loomes, T. N. Kitsopoulos, A. Brown, G. G. Balint-Kurti, O. S. Vasyutinskii, and J. A. Beswick, Science 300, 1936 (2003).
- [20] D. Sofikitis, C. S. Kannis, G. K. Boulogiannis, and T. P. Rakitzis, Phys. Rev. Lett. 121, 083001 (2018).
- [21] A. K. Spiliotis, M. Xygkis, M. E. Koutrakis, K. Tazes, G. K. Boulogiannis, C. S. Kannis, G. E. Katsoprinakis, D. Sofikitis, and T. P. Rakitzis, Light Sci. Appl. 10, 35 (2021).
- [22] T. Sun, Q. Zhao, F. Wan, Y. I. Salamin, and J.-X. Li, Phys. Rev. Lett. 132, 045001 (2024).
- [23] M. Wen, M. Tamburini, and C. H. Keitel, Phys. Rev. Lett. 122, 214801 (2019).
- [24] S. Bohlen, Z. Gong, M. J. Quin, M. Tamburini, and K. Põder, Phys. Rev. Res. 5, 033205 (2023).

- [25] Y. Wu, L. Ji, X. Geng, Q. Yu, N. Wang, B. Feng, Z. Guo, W. Wang, C. Qin, X. Yan et al., New J. Phys. 21, 073052 (2019).
- [26] T. Rakitzis, P. Samartzis, R. Toomes, L. Tsigaridas, M. Coriou, D. Chestakov, A. Eppink, D. Parker, and T. Kitsopoulos, Chem. Phys. Lett. 364, 115 (2002).
- [27] D. Sofikitis, P. Glodic, G. Koumarianou, H. Jiang, L. Bougas, P. C. Samartzis, A. Andreev, and T. P. Rakitzis, Phys. Rev. Lett. 118, 233401 (2017).
- [28] D. Sofikitis, M. G. Stamatakis, D. G. Papazoglou, and T. P. Rakitzis, Front. Phys. 12, 1480868 (2024).
- [29] G. G. Balint-Kurti, A. J. Orr-Ewing, J. A. Beswick, A. Brown, and O. S. Vasyutinskii, J. Chem. Phys. 116, 10760 (2002).
- [30] A. K. Spiliotis, M. Xygkis, M. E. Koutrakis, D. Sofikitis, and T. P. Rakitzis, Chem. Phys. Impact 2, 100022 (2021).
- [31] J. Fox and E. Gal, Proc. Phys. Soc. 90, 55 (1967).
- [32] P. S. Krstic and D. R. Schultz, Nucl. Fusion Suppl. 8 (1999).
- [33] P. S. Krstic and D. R. Schultz, J. Phys. B: At., Mol. Opt. Phys. 32, 3485 (1999).
- [34] A. Pukhov, J. Plasma Phys. 61, 425 (1999).
- [35] A. Pukhov, Proc. 2014 CAS-CERN Accel. School: Plasma Wake Accel. 1, 181 (2016).
- [36] A. Pukhov, J. Comput. Phys. 418, 109622 (2020).
- [37] E. Brunetti, R. N. Campbell, J. Lovell, and D. A. Jaroszynski, Sci. Rep. 12, 6703 (2022).
- [38] D. Papp, J. C. Wood, V. Gruson, M. Bionta, J.-N. Gruse, E. Cormier, Z. Najmudin, F. Legare, and C. Kamperidis, Nucl. Instrum. Methods Phys. Res. A 909, 145 (2018).
- [39] M. Klaiber, E. Yakaboylu, C. Müller, H. Bauke, G. G. Paulus, and K. Z. Hatsagortsyan, J. Phys. B: At., Mol. Opt. Phys. 47, 065603 (2014).
- [40] S. Steinke, J. Van Tilborg, C. Benedetti, C. Geddes, C. Schroeder, J. Daniels, K. Swanson, A. Gonsalves, K. Nakamura, N. Matlis *et al.*, Nature (London) **530**, 190 (2016).
- [41] C. A. Lindstrøm, Phys. Rev. Accel. Beams 24, 014801 (2021).
- [42] J. Thomas, A. Hützen, A. Lehrach, A. Pukhov, L. Ji, Y. Wu, X. Geng, and M. Büscher, Phys. Rev. Accel. Beams 23, 064401 (2020).
- [43] Z. Gong, M. J. Quin, S. Bohlen, C. H. Keitel, K. Põder, and M. Tamburini, Matter Radiat. Ext. 8, 064005 (2023).
- [44] T. Čižmár and K. Dholakia, Opt. Express 17, 15558 (2009).
- [45] A. Sharma, Z. Tibai, J. Hebling, and J. A. Fulop, J. Phys. B: At., Mol. Opt. Phys. 51, 204001 (2018).
- [46] E. A. Nanni, W. R. Huang, K.-H. Hong, K. Ravi, A. Fallahi, G. Moriena, R. Dwayne Miller, and F. X. Kartner, Nature Commun. 6, 8486 (2015).